Higher Order Temperature to Polarization Leakage Analysis of BICEP3 Beam Maps Using Shapelets with Applications to CMB-S4

Eli Meisel
Advisor: Colin Bischoff
University of Cincinnati Physics Department

December 6, 2023

Abstract

Temperature to polarization leakage is one way for systematic noise to be interpreted as a real signal. Using 'shapelets', we parameterize beam maps from BICEP3. Detectors come in pairs and the pair difference shows the temperature to polarization leakage. We simulated temperature to polarization leakage from the differential shapelet coefficients at different expansion orders. Statistical distributions of shapelet parameters were used to create potential CMB-S4 beams for further analysis.

1 Background

The theory of inflation says that at the time of the big bang, the universe grew exponentially [1]. This sudden growth created primordial gravitational waves (PGW) and perturbations in the density of matter. When the universe started cooling, it became transparent and light was free to move, it redshifted into the microwave part of the spectrum creating what is now called the cosmic microwave background (CMB). Within the CMB, there are tiny temperature fluctuations in different areas which show the different densities of matter meaning a less homogeneous early universe. If present, PGWs can be seen in the CMB, with the B-mode polarization being the best way to see this. Specifically, the PGW create both even parity (E-mode) and odd parity (B-mode) polarization [2]. But at this stage of the universe, B-modes are only created with gravitational waves. Detecting these B-modes proves the existence of these PGW which gives strong evidence for the theory of inflation . BICEP3's primary objective is to look for PGWs by making deep polarization maps at 95GHz to detect B-modes. Located at Amundsen-Scott South Pole Station, BICEP3 has a field of view of 27.4°, an aperture of 520mm in diameter, and houses 2560 detectors total [3]. Each detector comes in a pair of 'A' and 'B' beams where A and B are orthogonally polarized. Temperature to polarization leakage occurs when a pair difference is sensitive to unpolarized fluctuations. If we get this leakage when paired beams don't match, then the unpolarized perturbations give different responses for one beam than the other [4]. Since the CMB temperature fluctuations are orders of magnitude brighter than B-modes, even a small amount of temperature to polarization leakage can be a major problem.

Our goal for this project was to analyze BICEP3 beams and create simulations of possible CMB-S4 beams for leakage analysis. This paper starts by outlining the parameterization of BICEP3 beams in section 2 and how this model interacts with beam maps in section 3. Section 4 goes through the accuracy of the parameterization and the noise associated with BICEP3 beam maps. Lastly, section 5 shows the simulation of CMB-S4 beam maps and temperature to polar-

ization leakage analysis.

2 Shapelets

The method for image analysis called 'shapelet' expansion [5] is very useful for parameterizing BICEP3 beam maps. 1D shapelets are analogous to solutions to the quantum harmonic oscillator. They are the perturbations around a Gaussian function. The shapelet basis function can be represented with

$$\Phi_n(x) \equiv [2^n \pi^{\frac{1}{2}} n!]^{-\frac{1}{2}} H_n\left(\frac{x}{\sigma}\right) e^{-\frac{x^2}{2\sigma}} \qquad (1)$$

where $H_n(x)$ are Hermite polynomials, σ is the Gaussian width, and n is the expanded order number.

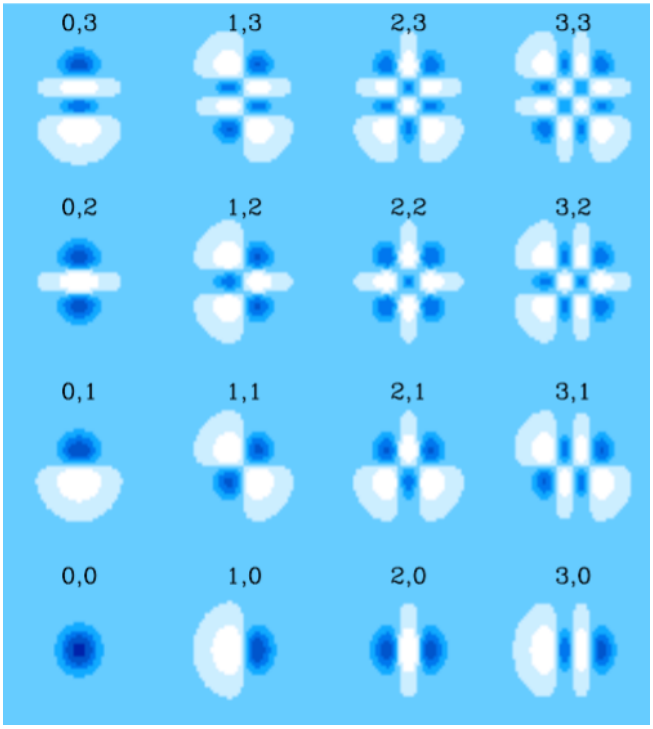

Figure 1: 2-dimensional shapelet beams [5], numbers above shape corresponds to (n1,n2). Orders are read diagonally (top left to bottom right) starting with order 0 with (0,0) then order 1 with (0,1) and (1,0) and so on. The 0th order is a Gaussian. The first order is a dipole shape. The second order has a quadrapole shape for the cross term.

These are orthonormal, so

$$\int_{-\infty}^{\infty} dx \Phi_n(x) \Phi_m(x) = \delta_{nm}, \qquad (2)$$

where δ_{nm} is the Kronecker delta. 2D shapelets are the tensor product of 2 Phi functions

$$\Phi_{n_1 n_2} \equiv \Phi_{n_1}(x) \Phi_{n_2}(y) \qquad (3)$$

Figure 1 shows individual basis functions of these shapelets.

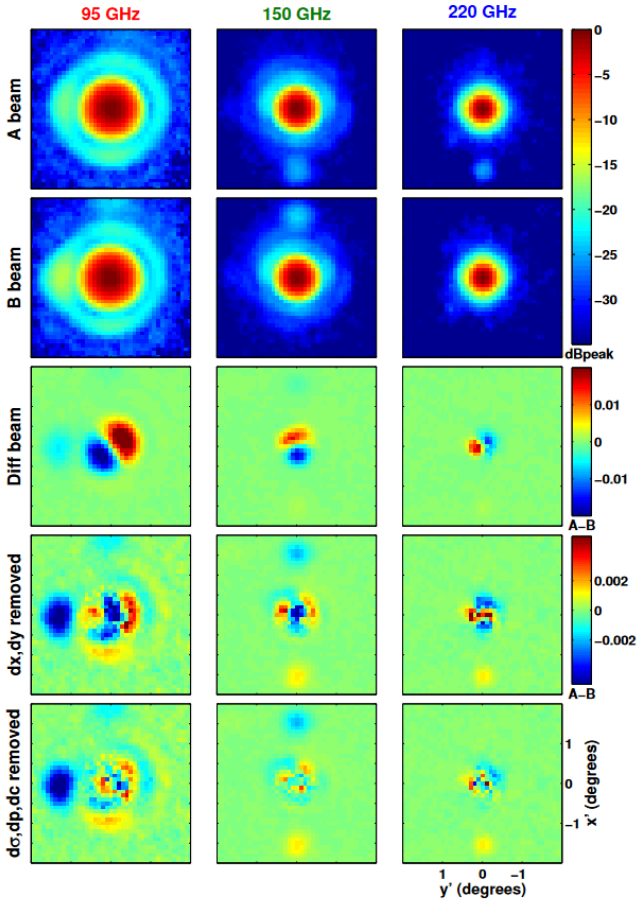

Figure 2: Far field beam maps taken with BICEP2 and Keck Array [4]. The top two rows show the A and B beams with the 95GHz signal from the Keck array and the 150GHz and 220GHz signals from BICEP2. The third row shows the differential beam. The fourth row shows the result of the first deprojection which takes away the equivalent of order 1. The final row shows the second deprojection which removes orders 1 and 2. Any secondary beam, noncircular beam, or Airy rings can be attributed to crosstalk.

Beam maps from BICEP3 look approximately Gaussian. Shapelets approximate this beam shape for a convenient parametrization. Unlike previous methods of analysis, the use of shapelets allows for a higher order analysis of

beams and how T→P leakage effects B-mode power spectra. Previous analysis used a deprojection technique [4] which analyzed to the equivalent of order 2. Figure 2 shows the results of deprojection. The top two rows show the A and B beams with the 95GHz signal from the Keck array and the 150GHz and 220GHz signals from BICEP2. The third row shows the A-B beam. The fourth row shows the result of the first deprojection which takes away the equivalent of order 1. The final row shows the second deprojection which removes orders 1 and 2. Calculation of T→P leakage is possible. However, for a deeper analysis on any leakage present, higher orders are needed. Our analysis tackles the higher order terms that haven't been analyzed previously. Shapelets present a convenient parametrization to approximate the beam shape and show how the A and B beams differ from one another.

3 BICEP3 analysis

The BICEP3 beams are comprised of 935 working detector pairs. All coefficients from orders 1+ have been normalized by their order 0 coefficients. To obtain the coefficients, a linear regression was used in conjunction with the shapelets with each order and permutation done separately. The following sections go though parameter optimization for the linear regression and the results of the BICEP3 higher order analysis.

3.1 Shapelet decomposition of BICEP3 Beams

For the decomposition on BICEP3 beam maps, we used a linear regression. Since the shapelet bases are orthonormal, the result is what we call the coefficient.

$$a_{ij} = \Omega \sum_{pixels} (Beam)\Phi_{ij} \tag{4}$$

where a_{ij} is the coefficient, i and j are the permutation values, and Ω is the solid angle. A beam can be created using

$$Beam = \sum_{ij} a_{ij}\Phi_{ij} \tag{5}$$

This is repeated with all orders using a coefficient from a normal distribution with standard deviation of 0.4. The results can be seen in figure 3. Each order looks like their (order, 0) counterpart from figure 1.

3.2 Beam Centralization

Not all BICEP3 beams are centered at the exact center of the grid. While this on its own isn't a problem, it becomes a problem when analyzing the beams using the method of linear regression. Since Φ_{ij} can be centered anywhere, making sure its center matched the center of the BICEP3 beam maps was crucial for accurate coefficient measurements. We started by calculating the order 1 coefficients from BICEP3 beams using the nominal center position model shown in equation 6.

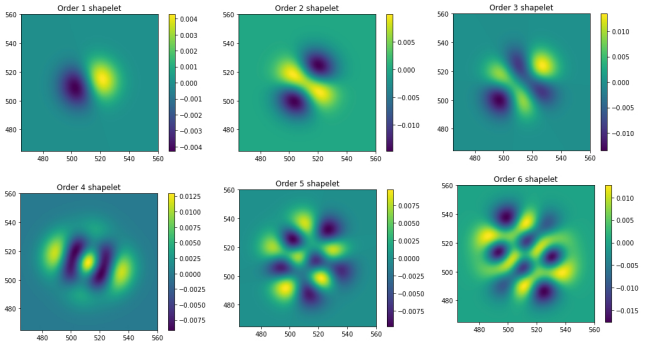

Figure 3: Example BICEP3 shapelets, orders 1-6. These were created using a basic shapelet function together with coefficients from a normal distribution. They all look like their (order, 0) counterparts from figure 1. The axes are in units of pixels which are 0.05 degrees.

$$\Phi_{ij}(x - x_0) = [2^n \pi^{\frac{1}{2}} n!]^{-\frac{1}{2}} H_n\left(\frac{x - x_0}{\sigma}\right) e^{-\frac{(x-x_0)^2}{2\sigma}} \tag{6}$$

where x_0 is the center of the grid. Order 1 was used because it changes the x and y center position of the shapelet. These coefficients were taken with the aim of minimizing them. The center was measured for each detector pair and the average was used for both the A and B beams in that pair. This calculation occurred for each pair. A consequence of this is that the (0,1)

and (1,0) coefficients become completely anticorrelated (this will come up in section 5.1). The results showed around a half-pixel deviation from the edge of the pixel in both the x and y directions.

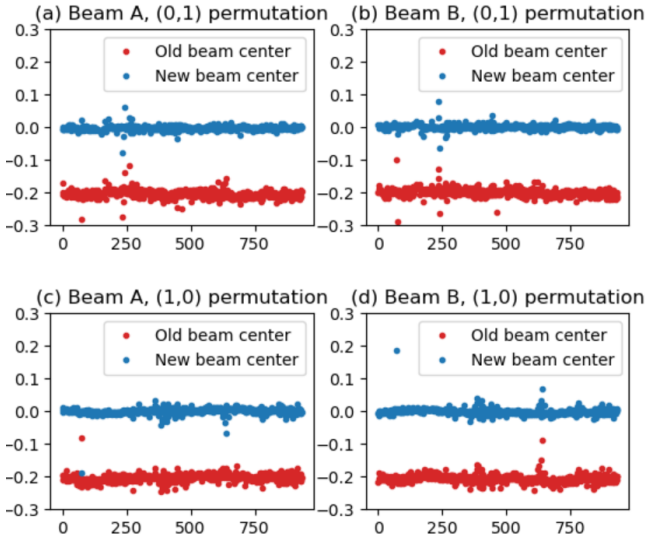

Figure 4: Order 1 coefficients for beam without changing the center (old pictured in red) and with the change (new pictured in blue). The x axis is the detector number and the y axis is the coefficients for (0,1) and (1,0) added together. The coefficients are substantially closer to 0 for both beams and permutations.

Figure 4 shows the center change coefficients for the (0,1) permutation and the (1,0) permutation. By design, the coefficients should be (or close to) 0 since that was one of the parameters for picking the new center. The coefficients for the order 1 permutations are substantially closer to 0 for both beams.

3.3 Beam size

Similarly to section 3.2, each detector pair has a slightly different beam width so the shapelet model needs to be adjusted. To find the best beam width, a range of beam sizes from 0.15-0.18 degrees was applied. Order 2 coefficients were used because this change affects the results the most in orders 1 and 2 since they are the orders with the most real signal. In addition, using order 1 coefficients for both the beam center parameter and for the beam size parameter would lead more error in the measurement. Order 2 coefficients (0,2) and (2,0) were averaged across the detector pair and fit to a polynomial. The beam width associated with the minimum of this function was used as the beam size for the pair of detectors. We did this for each pair individually for the most accurate coefficients. The average beam size was 0.172 degrees.

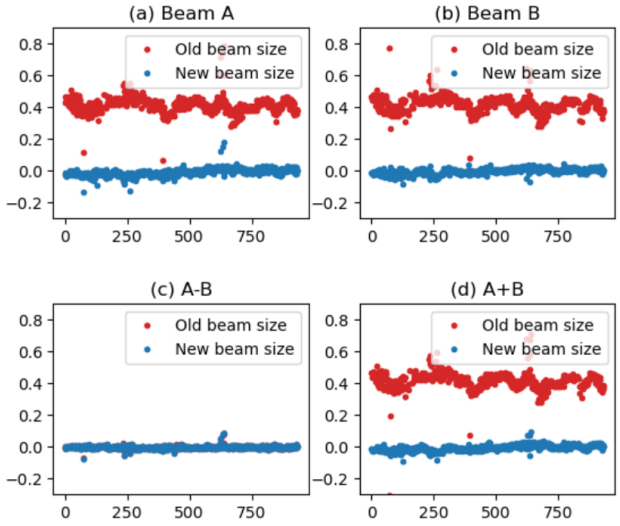

Figure 5: Beam size change plots. The x axis is the detector number and the y axis is the coefficients from (0,2) and (2,0) added together. In red is the old beam where no change has been made to the size of Phi and in blue is the beam with the size change. Results show a decrease in outliers that previously caused histograms to favor one permutation over another. The old beam has more variation in the coefficients and is farther from 0.

Figure 5 shows the before and after results. Histograms (not present, though results may be seen in section 3.4) were created showing the distribution of coefficients for each detector for each permutation. Results from these statistic histograms showed a decrease in outliers that previously caused histograms to favor one permutation over another. The old beam has more variation in the coefficients and is farther from 0. One of the criteria was for the coefficients to be 0 for that beam size to be chosen which can be seen for each plot. Overall, the A and B coefficients decreased substantially toward 0 and become more consistent with one another which means the model's parameters are closer to the

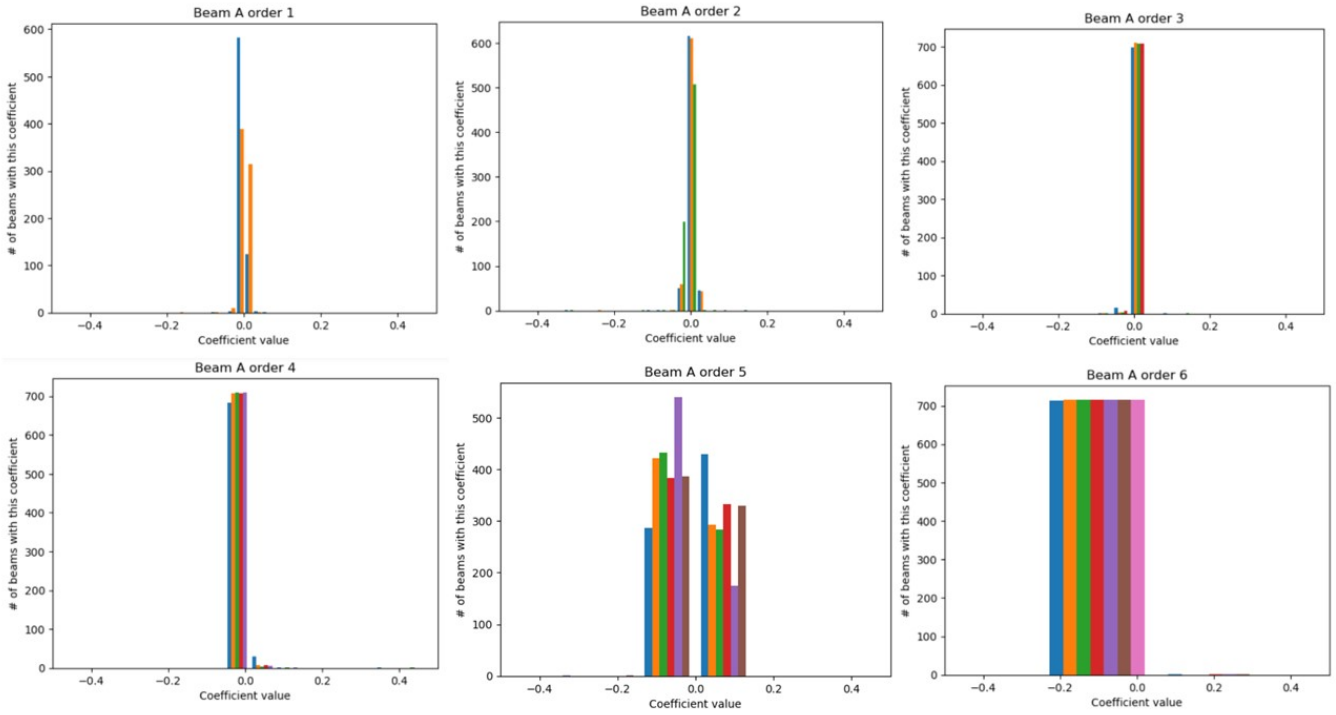

Figure 6: Beam A coefficients. The different colors represent different permutations. The spread is concentrated around 0 but slightly negative for order 1. This is a product of section 3.2. The higher orders show a larger spread and a consistent coefficient value pointing to a noise dominated beam.

beam maps. These improvements help the estimates of shapelet coefficients.

3.4 Beam analysis

With the shapelet parameter changes mentioned in the previous sections, we can now analyze BICEP3 beams for their coefficients. The distributions for the A and B beams can be seen in figure 6 and figure 7. The distribution for the differential A-B beam can be seen in figure 8. Any coefficient in this figure that isn't 0 means there is some differences that cause leakage. Most differences happen as the order increases which also suggests the presence of noise and lack of a real signal.

Most coefficients hover around 0 with some exceptions for order 1 and order 2 (which, as stated in section 3.3 and section 3.2, are there by design and therefore expected). As the order increases, so does the width of the distribution and the consistency of the coefficient value, pointing to noise becoming increasingly overwhelming over a real signal. The higher order consistency of coefficients also means there are less unique beams because the amount of real signal decreases.

4 Accuracy and noise analysis

4.1 Accuracy of shapelet model

Shapelets are convenient, but are they accurate? Using coefficients from BICEP3, we created simulations of beams and found their coefficients using the same method as section 3.4 to compare with the real beam maps. These simulated beam's coefficients were subtracted from the BICEP3 beam's coefficients to calculate the fractional error coming from the shapelet model. The goal for these calculations were to test the possible information loss due to the pixel size.

Figure 9 shows the results. The x-axis is the order and the y-axis is the fractional error. Expectantly, as order increases, so does the error. The coefficients can still be recovered from or-

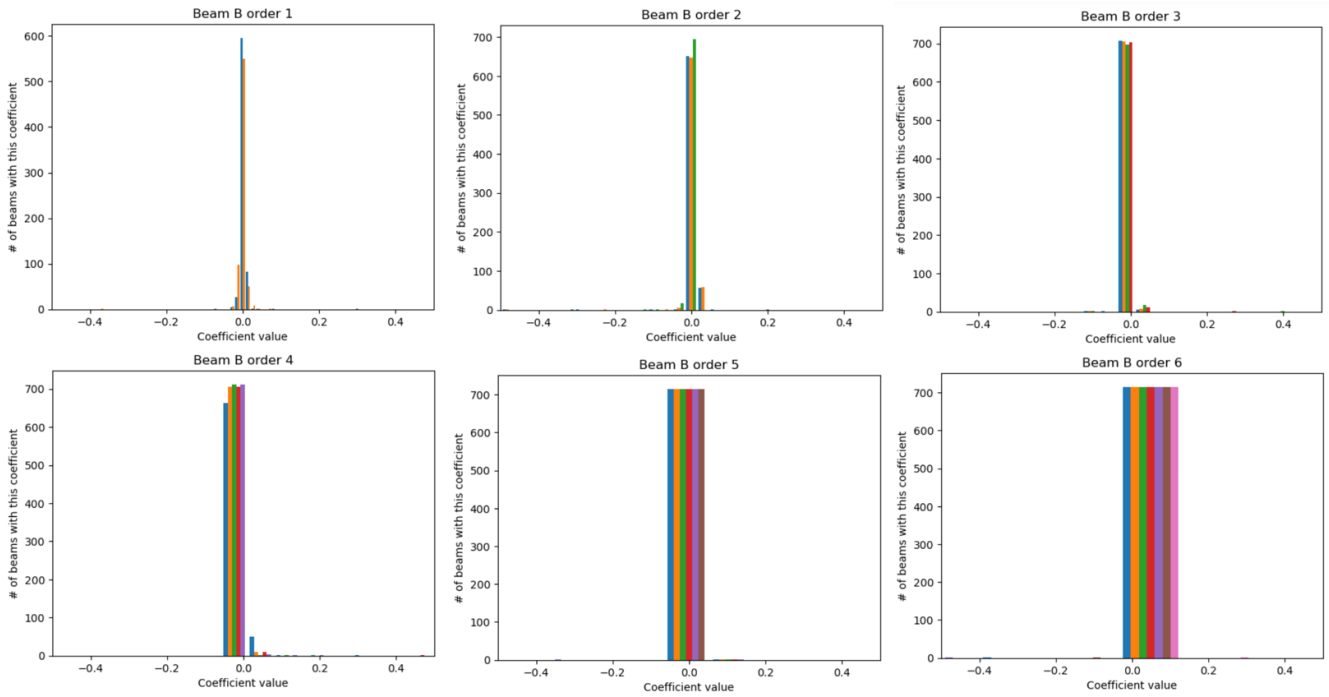

Figure 7: Beam B coefficients. The different colors represent different permutations. Similar to the beam A coefficients, order 1 is slightly negative and the spread for higher orders is wider than the lower orders which points to a noise or leakage dominated beam. Beam B coefficients being similar to beam A is expected since they are ideally the exact same beam.

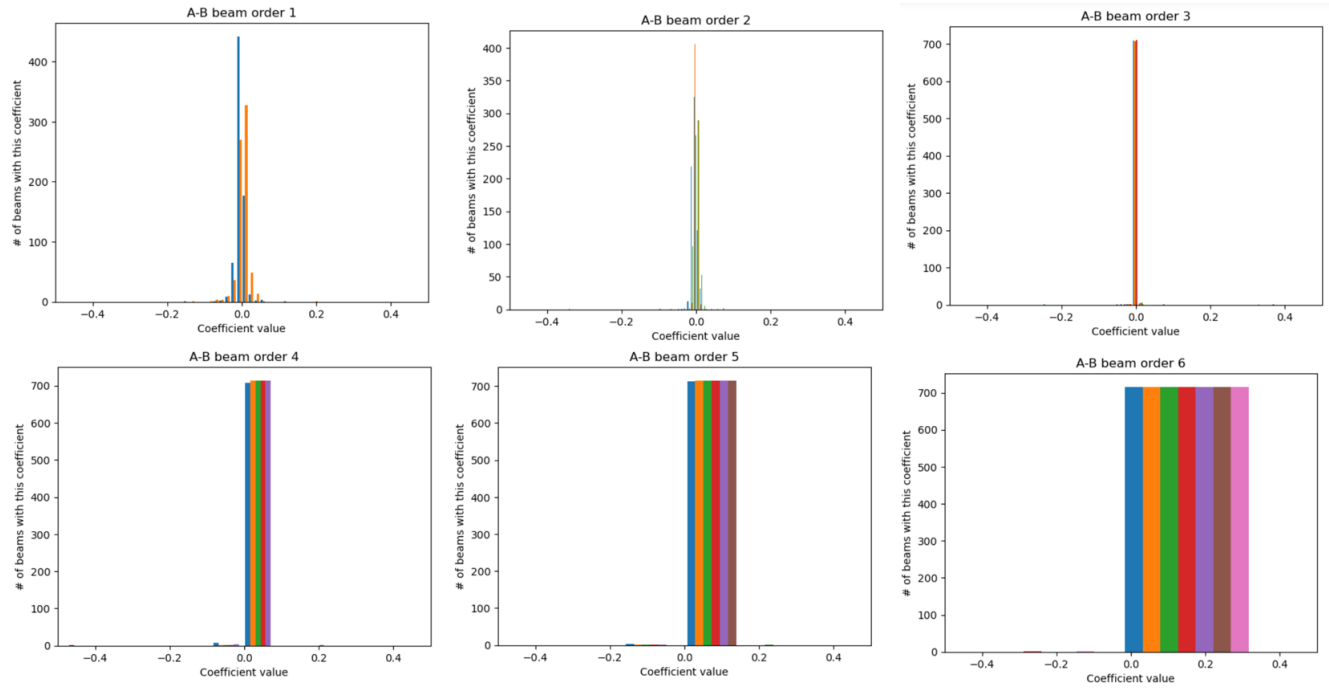

Figure 8: A-B coefficients. The different colors represent different permutations. The coefficients are centered around 0. Here, if a coefficient is not 0, then there is some difference between the A and B beams which is the cause of leakage. The higher orders largely have the same coefficient showing that each detector

der 10 but we stopped at order 6 for our analysis since there didn't seem to be much difference be-

tween the higher orders. This information loss is one of the main reasons our analysis stopped at order 6. The fractional error was sufficiently low for the lower orders that we were confident that the shapelet model is a good descriptor of BICEP3 beam maps and that our results could be trusted.

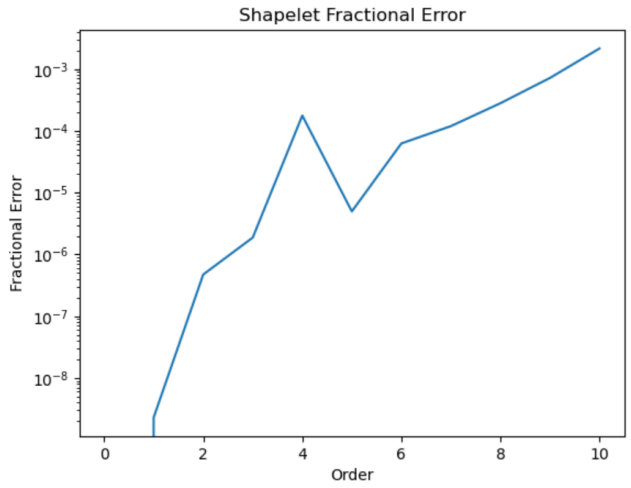

Figure 9: Shapelet fractional error. The x-axis is the order and y-axis is the fractional error. Expectantly, as order increases, so does the error. The coefficients can still be recovered from order 10. We stopped at order 6 for our analysis since there didn't seem to be much difference between the higher orders. Additionally, the higher orders are more difficult to get accurate coefficients from because of the amount of pixels available.

4.2 Noise analysis

With any data taken with a physical instrument, there is noise. To measure the amount of noise present, we started with a basic shapelet with a random coefficients from a normal distribution with a 5 percent deviation from the center. This would act as a noiseless beam map. Then we calculated the overall noise standard deviation from the BICEP3 beams by finding the coefficients in an area of the beam map with no signal which came out to $4.04 * 10^{-5}$ (value with arbitrary units). This value was used for the standard deviation for a simulated noise beam. Since higher orders for this shapelet don't exist, any results from higher orders is noise.

Figure 10 show the recovered coefficients for the noise beam. After using a linear regression (like in section 3.4), the results showed Gaussian distribution curves. All orders and permutations within each order follow a normal distribution with similar standard deviations of $4 * 10^{-6}$. The white noise distribution is similar across all orders and permutations as expected since noise shouldn't change across orders.

5 CMB-S4 Simulations

5.1 Gathering BICEP3 parameter statistics for CMB-S4 simulations

Creating simulations for CMB-S4 will show potential beams and now much leakage is occurring if the current specifications of detectors stay the same. With our leakage analysis tool, any new beams using experimental versions of new detectors can be analyzed for leakage. To create CMB-S4 simulations, the statistics for BICEP3 beams need to be found first. Each permutation would pull from a separate distribution corresponding to that permutation and would be used for each detector pair. The first step is to characterize the BICEP3 coefficient distributions; the variance of each distribution and the covariance. The general equation for the variance of a data set is

$$\begin{aligned} Var(A-B) &= <(A-B)^2> - <A-B>^2 \\ &= <A^2> + <B^2> - 2<AB> \end{aligned} \tag{7}$$

where

$$\begin{aligned} A &= \sigma_A^2 + \sigma_{AN}^2 \\ B &= \sigma_B^2 + \sigma_{BN}^2 \end{aligned} \tag{8}$$

For equation 7), we also assumed that $<A>=<B>=0$. σ is the standard deviation of the coefficient distribution and σ_A and σ_B are the intrinsic values, or values without noise, of the BICEP3 beam maps. Plugging σ_A and σ_B into equation 7 gives

$$Var(A-B) = \sigma_A^2 + \sigma_{AN}^2 + \sigma_B^2 + \sigma_{BN}^2 - 2<AB> \tag{9}$$

where σ_{AN} and σ_{BN} are the distributions from the noise beams found in section 4.2. For the covariance matrix, we need $<AB>$ which is found

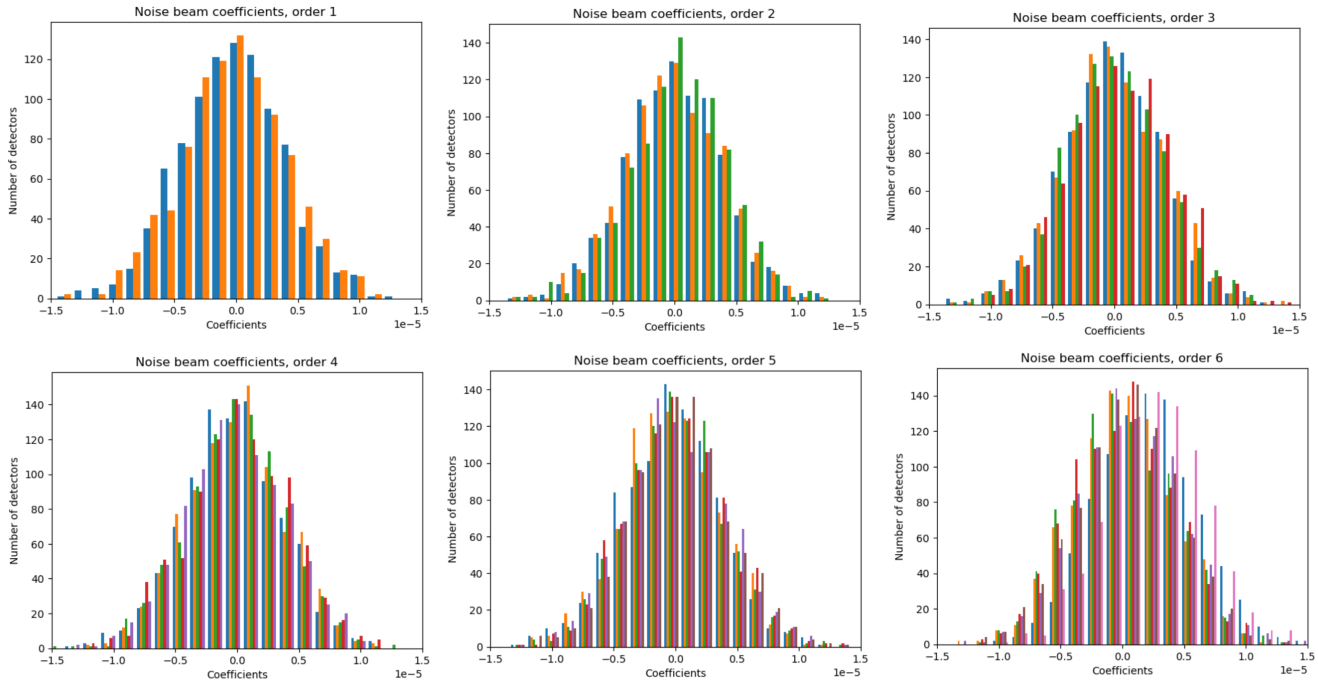

Figure 10: Noise analysis. Noise is stable across all orders as expected. The distributions also follow the same distribution for every permutation.

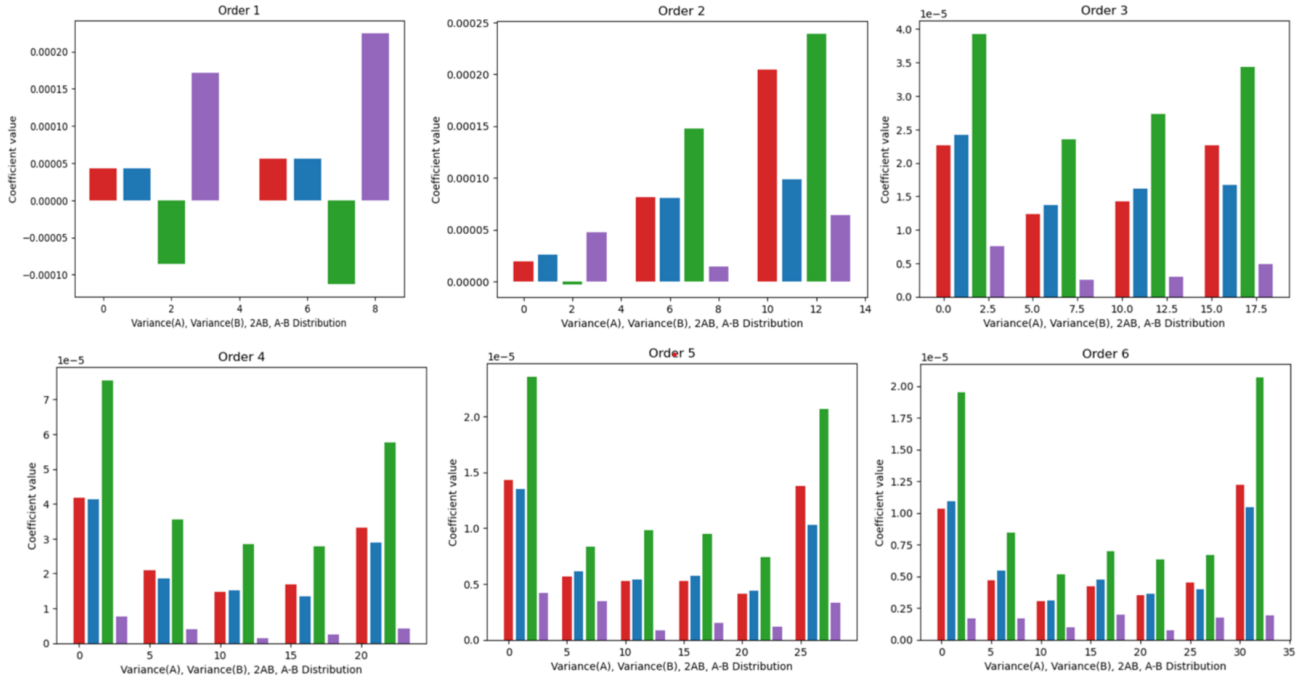

Figure 11: Histograms from each permutation. Each cluster of four bars represents one permutation. The far left group is the (0, order) permutation and continues to the right ending with the (order, 0) permutation. The first bar (red) in each group is σ_A^2, the second (blue) is σ_B^2, the third (green) is the correlation between σ_A and σ_B (aka 2AB), and the fourth (purple) is distribution of A-B. 2AB is negative for order 1 because A and B are totally uncorrelated due to methods used in sections 3.3 and 3.2. Overall, 2AB is much higher in the (0,order) and (order,0) permutations. This could be caused by a strictly horizontal and vertical dipole dominance in the beam difference.

from rearranging equation 9. The covariance of

two parameters A and B is

$$C_{AB} = \frac{1}{2}AB \tag{10}$$

So the covariance matrix for BICEP3 is

$$CM_{AB} = \begin{bmatrix} \sigma_A^2 - \sigma_{AN}^2 & C_{AB} \\ C_{AB} & \sigma_B^2 - \sigma_{BN}^2 \end{bmatrix} \tag{11}$$

The general form for a 2D probability Gaussian function is

$$P(A,B) = N * \exp\left\{-\frac{1}{2} * \vec{x} C_{AB}^{-1} \vec{x}\right\} \tag{12}$$

where N is a normalization factor, C is the covariance matrix for beams A and B, and $\vec{x}$ is the coefficient values from A and B. The random coefficients are generated using a Cholesky decomposition of C. This became the model for the statistical distributions. The values of the BICEP3 statistics are shown in figure 11. Each cluster of four bars represents one permutation. The far left group is the (0, order) permutation and continues to the right ending with the (order, 0) permutation. The first bar (red) in each group is σ_A^2, the second (blue) is σ_B^2, the third (green) is the correlation between σ_A and σ_B (aka 2AB), and the fourth (purple) is distribution of A-B.

The covariance of the A and B beams is negative for order 1 because A and B are totally anticorrelated due to methods used in section 3.2. Overall, the covariance is much higher in the (0,order) and (order,0) permutations. This could be caused by a strictly horizontal and vertical dipole dominance in the beam difference. Therefore, the A-B distribution has a narrower width and the values are more correlated.

5.2 CMB-S4 Temperature to Polarization Leakage Analysis

The CMB-S4 simulations pulled coefficients from the distributions in the previous section. Because of the deprojecion technique mentioned in section 2, two simulations were created and analyzed. The first used the distributions for all orders and the second used the distributions from orders 3+. Figure 12 shows an example of a A-B difference beam from the first case and figure 13 shows an A-B difference beam from the second. The resolution is the same as the BICEP3 beams and the beam width is the average (see section 3.3) 0.172 degrees.

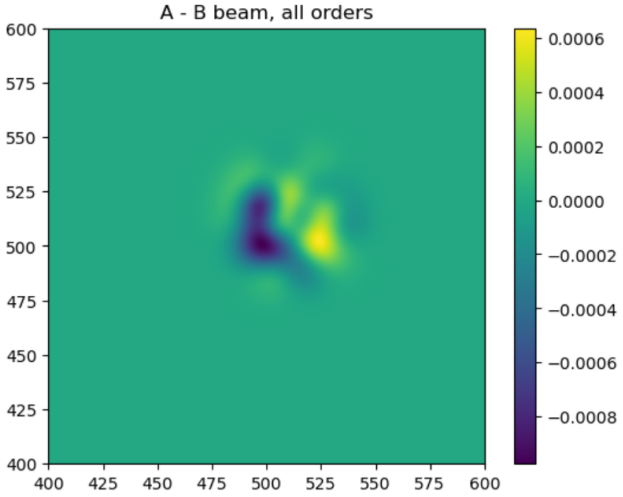

Figure 12: Example simulated difference beam made from BICEP3 statistics. The main shape present is a dipole showing an order 1 dominance.

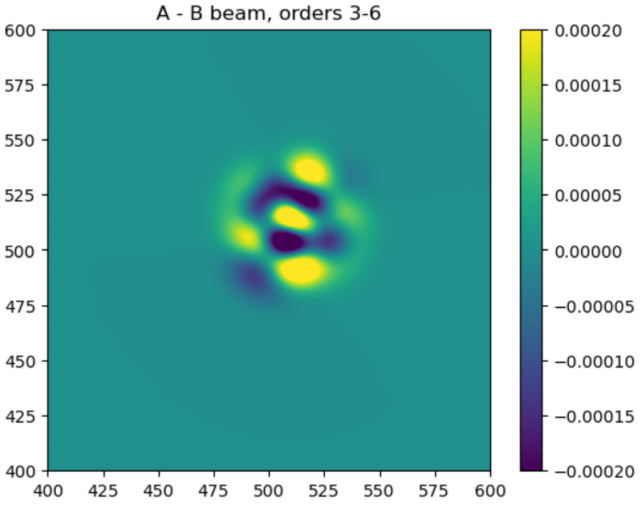

Figure 13: Example simulated difference beam without orders 1 and 2. The dominant shape shows 6 main lobes showing an orders 3 and 4 dominance.

For the first case, the difference beam is a clear dipole and shows an order 1 dominance as expected. The second case shows a more complicated shape and has more dominance in order 3 and order 4 which is expected because of the weirder shape. To find the temperature to B-mode polarization leakage from the S4 simulations, code from Alec Hrycuik [6] was used. The

code took in T (temperature), Q, and U beams (where Q and U are Stokes parameters for linear polarization). Using the differential shapelet coefficients, T→Q and T→U beams were created. T→Q and T→U represent the off diagonals and are created with an A+B beam. The Fourier transform of these gives T→B leakage and Q→Q and U→U give B→B beam transfer function. From here we took the ratio, T→B/B→B, of these to see how much of an impact temperature leakages had on the polarization.

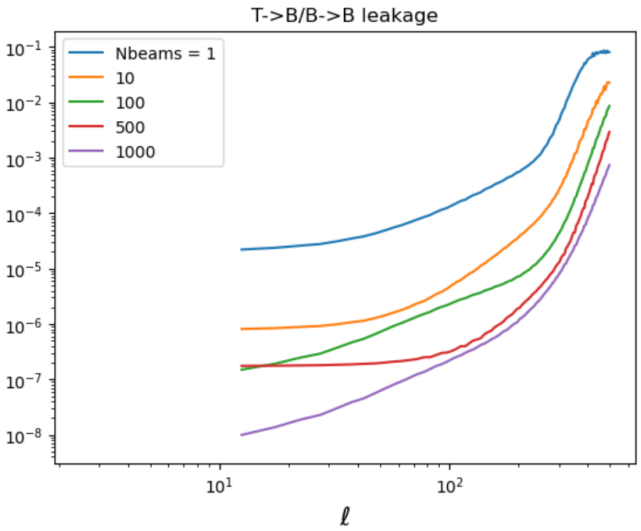

Figure 14: Temperature to B-Mode polarization leakage against ℓ for simulated beams from case one. Each line represents a different number of beams that was simulated. Blue is 1 beam, orange is 10, green is 100, red is 500, and purple is 1000. As the number of beams, n, increased, the leakage averaged down like 1/n.

The simulated T→B/B→B leakage plots are shown in figure 14 and figure 15. Each line represents a different number of beams that was analyzed. The simulations were created using 1, 10, 100, 500, and 1000 random simulated beams.

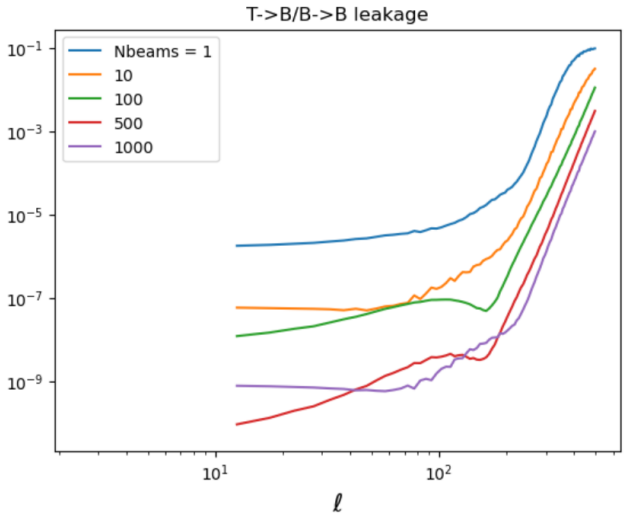

Figure 15: Temperature to B-Mode polarization leakage against ℓ for simulated beams from case two. Each line represents a different number of beams that was simulated. Blue is 1 beam, orange is 10, green is 100, red is 500, and purple is 1000. As the number of beams, n, increased, the leakage averaged down like 1/n. Compared to case one, these curves are more unstable.

As the number of beams, n, increased, the amount of leakage averaged down like 1/n. Compared to case one, case two's curves look more varied and cross over other curves. This was expected because the original beams that were used are more noise dominated and therefore more random and the difference beams would then have random perturbations creating more leakage.

6 Conclusion

The end goal of this project was to create simulations of future CMB-S4 beams for temperature to polarization leakage analysis. To achieve this, we had to analyze BICEP3 beam maps first. We used shapelets to parameterize the beams and used a linear regression to find the coefficients for the expanded beam. Statistics from the coefficients were used to create parameters used in the simulated beams. Then a Fourier Transform was performed to find the temperature to polarization leakage. Here, we found that as the number of beams increased, the amount of leakage averaged down like 1/n. The main gain that

came from our research was the tool used to analyze the temperature to polarization leakage in a given beam. It can also be used to discover what parameters would best minimize the effects of leakage in a physical detector.

References

[1] Eurpoean Space Agency, The Cosmic Microwave Background and Inflation, https://tinyurl.com/2s3ddf2n

[2] Kamionkowski and Kovetz, The Quest for B Modes from Inflationary Gravitational Waves, Annual Review of Astronomy and Astrophysics 2016 54:1, 227-269

[3] BICEP/Keck Collaboration. 2021, The Astrophysical Journal 927, 77 (2022), arXiv:2110.00482

[4] BICEP/Keck Collaboration. 2021, The Astrophysical Journal 884, 114 (2019), arXiv:1904.01640

[5] Refregier, A. 2001, Mon.Not.Roy.Astron.Soc.338:35,2003, arXiv:astro-ph/0105178

[6] Hrycuik, Alec. http://github.com/CMB-S4/map$_m ulti_t ool$